

000 054
 001 055
 002 056
 003 057
 004 058
 005 059
 006 060
 007 061
 008 062
 009 063
 010 064
 011 065
 012 066
 013 067
 014 068
 015 069
 016 070
 017 071
 018 072
 019 073
 020 074
 021 075
 022 076
 023 077
 024 078
 025 079
 026 080
 027 081
 028 082
 029 083
 030 084
 031 085
 032 086
 033 087
 034 088
 035 089
 036 090
 037 091
 038 092
 039 093
 040 094
 041 095
 042 096
 043 097
 044 098
 045 099
 046 100
 047 101
 048 102
 049 103
 050 104
 051 105
 052 106
 053 107

Supplementary File to “Multi-channel Weighted Nuclear Norm Minimization for Real Color Image Denoising”

Anonymous ICCV submission

Paper ID 572

In this supplementary file, we provide:

1. The proof of the Theorem 1 in the main paper.
2. More denoising results on the 24 high quality images from the Kodak PhotoCD dataset.
3. More visual comparisons of denoised images by different methods on the real noisy images of the dataset [1].
4. More visual comparisons of denoised images by different methods on the real noisy images of the dataset [2].

1. Proof of Theorem 1.

Theorem 1. Assume that the weights in w are in a non-descending order, the sequence $\{\mathbf{X}_k\}$, $\{\mathbf{Z}_k\}$, and $\{\mathbf{A}_k\}$ generated in Algorithm 1 satisfy:

$$(a) \lim_{k \rightarrow \infty} \|\mathbf{X}_{k+1} - \mathbf{Z}_{k+1}\|_F = 0; \quad (b) \lim_{k \rightarrow \infty} \|\mathbf{X}_{k+1} - \mathbf{X}_k\|_F = 0; \quad (c) \lim_{k \rightarrow \infty} \|\mathbf{Z}_{k+1} - \mathbf{Z}_k\|_F = 0. \quad (1)$$

Proof. 1. Firstly, we prove that the sequence $\{\mathbf{A}_k\}$ generated by Algorithm 1 is upper bounded. Let $\mathbf{X}_{k+1} + \rho_k^{-1} \mathbf{A}_k = \mathbf{U}_k \Sigma_k \mathbf{V}_k^\top$ be its singular value decomposition (SVD) [3] in the $(k+1)$ -th iteration. According to Corollary 1 of [4], we can have the SVD of \mathbf{Z}_{k+1} as $\mathbf{Z}_{k+1} = \mathbf{U}_k \hat{\Sigma}_k \mathbf{V}_k^\top = \mathbf{U}_k \mathcal{S}_{\frac{w}{\rho_k}}(\Sigma_k) \mathbf{V}_k^\top$. Then we have

$$\|\mathbf{A}_{k+1}\|_F = \|\mathbf{A}_k + \rho_k(\mathbf{X}_{k+1} - \mathbf{Z}_{k+1})\|_F = \rho_k \|\rho_k^{-1} \mathbf{A}_k + \mathbf{X}_{k+1} - \mathbf{Z}_{k+1}\|_F \quad (2)$$

$$= \rho_k \|\mathbf{U}_k \Sigma_k \mathbf{V}_k^\top - \mathbf{U}_k \mathcal{S}_{\frac{w}{\rho_k}}(\Sigma_k) \mathbf{V}_k^\top\|_F = \rho_k \|\Sigma_k - \mathcal{S}_{\frac{w}{\rho_k}}(\Sigma_k)\|_F \quad (3)$$

$$= \rho_k \sqrt{\sum_i (\Sigma_k^{ii} - \mathcal{S}_{\frac{w}{\rho_k}}(\Sigma_k^{ii}))^2} \leq \rho_k \sqrt{\sum_i \left(\frac{w_i}{\rho_k}\right)^2} = \sqrt{\sum_i w_i^2}. \quad (4)$$

The inequality in the second last step can be proved as follows: given the diagonal matrix Σ_k , we define Σ_k^{ii} as the i -th element of Σ_k^{ii} . If $\Sigma_k^{ii} \geq \frac{w_i}{\rho_k}$, we have $\mathcal{S}_{\frac{w}{\rho_k}}(\Sigma_k^{ii}) = \Sigma_k^{ii} - \frac{w_i}{\rho_k} \geq 0$. If $\Sigma_k^{ii} < \frac{w_i}{\rho_k}$, we have $\mathcal{S}_{\frac{w}{\rho_k}}(\Sigma_k^{ii}) = 0 < \Sigma_k^{ii} + \frac{w_i}{\rho_k}$. After all, we have $|\Sigma_k^{ii} - \mathcal{S}_{\frac{w}{\rho_k}}(\Sigma_k^{ii})| \leq \frac{w_i}{\rho_k}$ and hence the inequality holds true. Hence, the sequence $\{\mathbf{A}_k\}$ is upper bounded.

2. Secondly, we prove that the sequence of Lagrangian function $\{\mathcal{L}(\mathbf{X}_{k+1}, \mathbf{Z}_{k+1}, \mathbf{A}_k, \rho_k)\}$ is also upper bounded. Since the global optimal solution of \mathbf{X} and \mathbf{Z} in corresponding subproblems, we always have $\mathcal{L}(\mathbf{X}_{k+1}, \mathbf{Z}_{k+1}, \mathbf{A}_k, \rho_k) \leq \mathcal{L}(\mathbf{X}_k, \mathbf{Z}_k, \mathbf{A}_k, \rho_k)$. Based on the updating rule that $\mathbf{A}_{k+1} = \mathbf{A}_k + \rho_k(\mathbf{X}_{k+1} - \mathbf{Z}_{k+1})$, we have $\mathcal{L}(\mathbf{X}_{k+1}, \mathbf{Z}_{k+1}, \mathbf{A}_{k+1}, \rho_{k+1}) = \mathcal{L}(\mathbf{X}_{k+1}, \mathbf{Z}_{k+1}, \mathbf{A}_k, \rho_k) + \langle \mathbf{A}_{k+1} - \mathbf{A}_k, \mathbf{X}_{k+1} - \mathbf{Z}_{k+1} \rangle + \frac{\rho_{k+1} - \rho_k}{2} \|\mathbf{X}_{k+1} - \mathbf{Z}_{k+1}\|_F^2 = \mathcal{L}(\mathbf{X}_{k+1}, \mathbf{Z}_{k+1}, \mathbf{A}_k, \rho_k) + \frac{\rho_{k+1} + \rho_k}{2\rho_k^2} \|\mathbf{A}_{k+1} - \mathbf{A}_k\|_F^2$. Since the sequence $\{\|\mathbf{A}_k\|_F\}$ is upper bounded, the sequence $\{\|\mathbf{A}_{k+1} - \mathbf{A}_k\|_F\}$ is also upper bounded. Denote by a the upper bound of $\{\|\mathbf{A}_{k+1} - \mathbf{A}_k\|_F\}$, we have $\mathcal{L}(\mathbf{X}_{k+1}, \mathbf{Z}_{k+1}, \mathbf{A}_{k+1}, \rho_{k+1}) \leq \mathcal{L}(\mathbf{X}_1, \mathbf{Z}_1, \mathbf{A}_0, \rho_0) + a \sum_{k=0}^{\infty} \frac{\rho_{k+1} + \rho_k}{2\rho_k^2} = \mathcal{L}(\mathbf{X}_1, \mathbf{Z}_1, \mathbf{A}_0, \rho_0) + a \sum_{k=0}^{\infty} \frac{\mu+1}{2\mu^k \rho_0} \leq \mathcal{L}(\mathbf{X}_1, \mathbf{Z}_1, \mathbf{A}_0, \rho_0) + \frac{a}{\rho_0} \sum_{k=0}^{\infty} \frac{1}{\mu^{k-1}}$. The last inequality holds since $\mu+1 < 2\mu$. Since $\sum_{k=0}^{\infty} \frac{1}{\mu^{k-1}} < \infty$, the sequence of Lagrangian function $\{\mathcal{L}(\mathbf{X}_{k+1}, \mathbf{Z}_{k+1}, \mathbf{A}_{k+1}, \rho_{k+1})\}$ is upper bound.

3. Thirdly, we prove that the sequences of $\{\mathbf{X}_k\}$ and $\{\mathbf{Z}_k\}$ are upper bounded. Since $\|\mathbf{W}(\mathbf{Y} - \mathbf{X})\|_F^2 + \|\mathbf{Z}\|_{w,*} = \mathcal{L}(\mathbf{X}_k, \mathbf{Z}_k, \mathbf{A}_{k-1}, \rho_{k-1}) - \langle \mathbf{A}_k, \mathbf{X}_k - \mathbf{Z}_k \rangle - \frac{\rho_k}{2} \|\mathbf{X}_k - \mathbf{Z}_k\|_F^2 = \mathcal{L}(\mathbf{X}_k, \mathbf{Z}_k, \mathbf{A}_{k-1}, \rho_{k-1}) + \frac{1}{2\rho_k} (\|\mathbf{A}_{k-1}\|_F^2 - \|\mathbf{A}_k\|_F^2)$. Thus $\{\mathbf{W}(\mathbf{Y} - \mathbf{X}_k)\}$ and $\{\mathbf{Z}_k\}$ are upper bounded, and hence the sequence $\{\mathbf{X}_k\}$ is bounded by the Cauchy-Schwarz inequality

Table 1. PSNR(dB) results of different denoising methods on 24 natural images.

Image#	$\sigma_r = 5, \sigma_g = 30, \sigma_b = 15$								
	CBM3D	MLP	TNRD	NI	NC	WNNM-1	WNNM-2	WNNM-3	MC-WNNM
1	27.25	28.06	28.62	25.00	29.55	28.16	27.95	28.15	
2	29.70	31.30	32.70	27.80	29.69	32.54	31.60	31.73	
3	30.34	31.98	34.07	28.02	31.93	33.91	33.68	33.52	
4	29.47	31.10	32.56	27.70	32.56	32.68	31.85	31.90	
5	27.31	28.59	29.35	26.14	30.00	28.83	29.00	28.91	
6	28.20	29.10	29.90	26.15	28.81	29.55	29.46	29.62	
7	29.73	31.60	33.46	27.22	31.63	33.09	33.29	32.86	
8	27.47	28.16	28.91	25.34	30.16	29.15	29.24	29.03	
9	30.07	31.63	33.55	27.86	31.54	33.19	33.20	32.95	
10	29.96	31.37	33.20	27.74	33.44	32.98	33.02	32.74	
11	28.73	29.85	30.87	26.98	30.16	30.45	30.14	30.21	
12	30.20	31.50	33.31	27.97	31.69	33.22	32.71	32.65	
13	26.18	26.69	26.98	25.14	27.97	26.49	26.42	26.62	
14	27.86	29.07	29.87	26.67	29.21	29.36	29.14	29.30	
15	29.91	31.58	33.13	28.04	31.17	33.22	32.34	32.36	
16	29.29	30.35	31.54	27.46	32.18	31.34	31.05	31.21	
17	29.50	31.09	32.52	27.81	32.80	32.09	32.00	31.85	
18	27.72	28.74	29.36	26.57	28.63	28.88	28.76	28.89	
19	28.98	30.18	31.35	27.25	29.79	31.34	30.77	30.95	
20	30.63	31.78	33.27	27.89	29.52	33.00	32.55	32.58	
21	28.50	29.58	30.54	26.86	31.71	30.02	30.03	30.03	
22	28.61	29.78	30.82	27.19	30.50	30.47	29.82	30.10	
23	30.60	32.66	35.06	28.17	32.82	34.72	34.37	33.94	
24	27.97	28.81	29.61	26.01	30.75	29.47	29.35	29.39	
Average	28.92	30.19	31.44	27.04	30.76	31.17	30.91	30.89	32.70

and triangle inequality. We can obtain that $\lim_{k \rightarrow \infty} \|\mathbf{X}_{k+1} - \mathbf{Z}_{k+1}\|_F = \lim_{k \rightarrow \infty} \rho_k^{-1} \|\mathbf{A}_{k+1} - \mathbf{A}_k\|_F = 0$ and the equation (a) is proved.

4. Then we can prove that $\lim_{k \rightarrow \infty} \|\mathbf{X}_{k+1} - \mathbf{X}_k\|_F = \lim_{k \rightarrow \infty} \|(\mathbf{W}^\top \mathbf{W} + \frac{\rho_k}{2} \mathbf{I})^{-1} (\mathbf{W}^\top \mathbf{W} \mathbf{Y} - \mathbf{W}^\top \mathbf{W} \mathbf{Z}_k - \frac{1}{2} \mathbf{A}_k) - \rho_k^{-1} (\mathbf{A}_k - \mathbf{A}_{k-1})\|_F \leq \lim_{k \rightarrow \infty} \|(\mathbf{W}^\top \mathbf{W} + \frac{\rho_k}{2} \mathbf{I})^{-1} (\mathbf{W}^\top \mathbf{W} \mathbf{Y} - \mathbf{W}^\top \mathbf{W} \mathbf{Z}_k - \frac{1}{2} \mathbf{A}_k)\|_F + \rho_k^{-1} \|\mathbf{A}_k - \mathbf{A}_{k-1}\|_F = 0$ and hence (b) is proved.

5. Finally, (c) can be proved by checking that $\lim_{k \rightarrow \infty} \|\mathbf{Z}_{k+1} - \mathbf{Z}_k\|_F = \lim_{k \rightarrow \infty} \|\mathbf{X}_k + \rho_k^{-1} \mathbf{A}_{k-1} - \mathbf{Z}_k + \mathbf{X}_{k+1} - \mathbf{X}_k + \rho_k^{-1} \mathbf{A}_{k-1} + \rho_k^{-1} \mathbf{A}_k - \rho_k^{-1} \mathbf{A}_{k+1}\|_F \leq \lim_{k \rightarrow \infty} \|\Sigma_{k-1} - \mathcal{S}_{w/\rho_{k-1}}(\Sigma_{k-1})\|_F + \|\mathbf{X}_{k+1} - \mathbf{X}_k\|_F + \rho_k^{-1} \|\mathbf{A}_{k-1} + \mathbf{A}_{k+1} - \mathbf{A}_k\|_F = 0$, where $\mathbf{U}_{k-1} \Sigma_{k-1} \mathbf{V}_{k-1}^\top$ is the SVD of the matrix $\mathbf{X}_k + \rho_{k-1} \mathbf{A}_{k-1}$. \square

2. More denoising results on the 24 high quality images from the Kodak PhotoCD dataset

In the main paper, we have given the PSNR results of the competing methods on the 24 high quality images from the Kodak PhotoCD dataset when the standard deviations of the additive white Gaussian noise (AWGN) are $\sigma_r = 40, \sigma_g = 20, \sigma_b = 30$ for R, G, B channels, respectively. Here we provide more denoising results on this dataset. In Tables ??-??, we give more PSNR results on these images when the noise standard deviations are $\sigma_r = 5, \sigma_g = 30, \sigma_b = 15$ in Table 1 and $\sigma_r = 30, \sigma_g = 10, \sigma_b = 50$ in Table 2, respectively. In Figures 4-??, we give the visual comparisons of the denoised images by different methods.

216

217

218

219

220

221

222

223

224

225

226

227

228

229

230

231

232

233

234

235

236

237

238

239

240

241

242

243

244

245

246

247

248

249

250

251

252

253

254

255

256

257

258

259

260

261

262

263

264

265

266

267

268

269

270

271

272

273

274

275

276

277

278

279

280

281

282

283

284

285

286

287

288

289

290

291

292

293

294

295

296

297

298

299

300

301

302

303

304

305

306

307

308

309

310

311

312

313

314

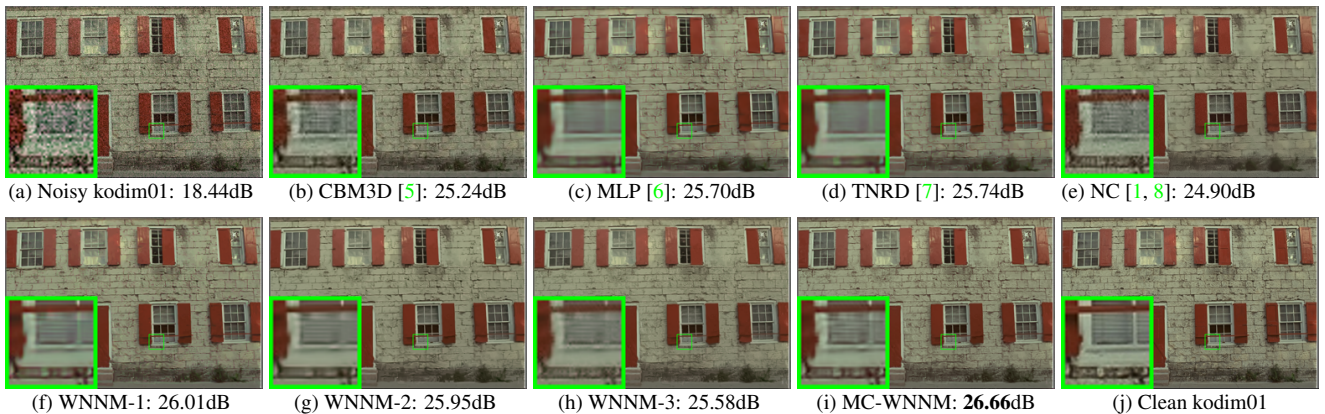
315

316

317

Table 2. PSNR(dB) results of different denoising methods on 24 natural images.

	$\sigma_r = 30, \sigma_g = 10, \sigma_b = 50$								
Image#	CBM3D	MLP	TNRD	NI	NC	WNNM-1	WNNM-2	WNNM-3	MC-WNNM
1	23.38	26.49	26.50	24.82	23.59	26.40	25.60		
2	25.19	30.94	30.90	26.82	27.79	30.89	29.75		
3	25.39	32.03	32.09	27.52	27.41	32.20	31.17		
4	24.96	30.55	30.47	27.34	27.00	30.74	29.71		
5	23.29	26.65	26.73	25.72	26.67	26.74	25.98		
6	24.09	27.76	27.70	26.10	26.12	27.85	26.96		
7	24.89	30.70	30.72	27.17	28.07	30.91	29.94		
8	23.30	26.12	26.27	25.59	26.11	26.87	26.33		
9	25.20	31.35	31.31	27.74	28.33	31.30	30.45		
10	25.13	31.01	31.05	27.60	28.53	31.12	30.17		
11	24.54	28.79	28.82	26.72	24.40	28.73	27.79		
12	25.43	31.60	31.60	27.82	29.01	31.59	30.62		
13	22.50	24.71	24.73	24.96	23.36	24.70	23.85		
14	23.91	27.69	27.72	26.26	23.08	27.62	26.81		
15	25.45	31.09	31.05	27.36	28.49	31.29	30.21		
16	24.89	29.79	29.73	27.35	27.10	29.84	28.85		
17	25.12	30.26	30.24	27.15	27.54	30.11	29.35		
18	23.83	27.26	27.26	26.05	26.15	27.32	26.18		
19	24.63	29.40	29.39	27.06	27.41	29.78	28.87		
20	26.43	31.16	31.27	26.43	26.92	31.25	30.43		
21	24.24	28.26	28.27	26.66	27.18	28.22	27.45		
22	24.51	29.03	29.06	26.83	27.64	29.02	27.81		
23	25.55	32.87	32.75	27.60	23.75	32.58	31.46		
24	23.85	27.06	27.13	25.86	27.05	27.50	26.63		
Average		24.57	29.27	29.28	26.69	26.61	29.36	28.43	29.90

Figure 1. Denoised images of different methods on the image ‘‘kodim01’’ degraded by AWGN with different standard deviations of $\sigma_r = 40, \sigma_g = 20, \sigma_b = 30$ on R, G, B channels, respectively. The images are better to be zoomed in on screen.

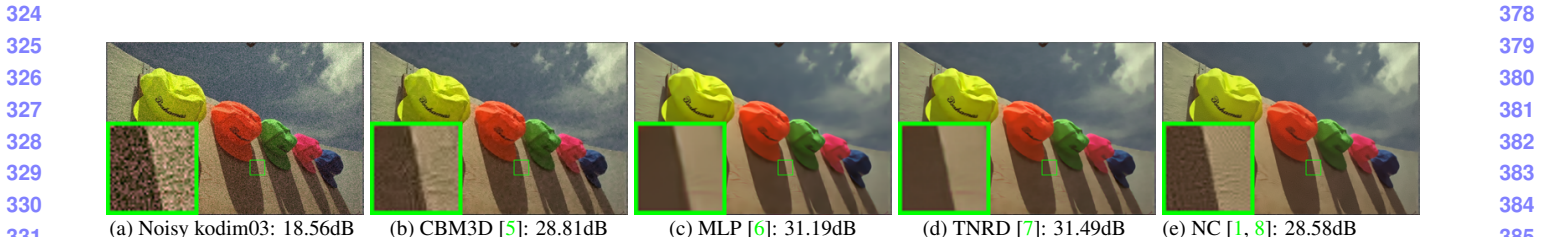


Figure 2. Denoised images of different methods on the image “kodim03” degraded by AWGN with different standard deviations of $\sigma_r = 40$, $\sigma_g = 20$, $\sigma_b = 30$ on R, G, B channels, respectively. The images are better to be zoomed in on screen.

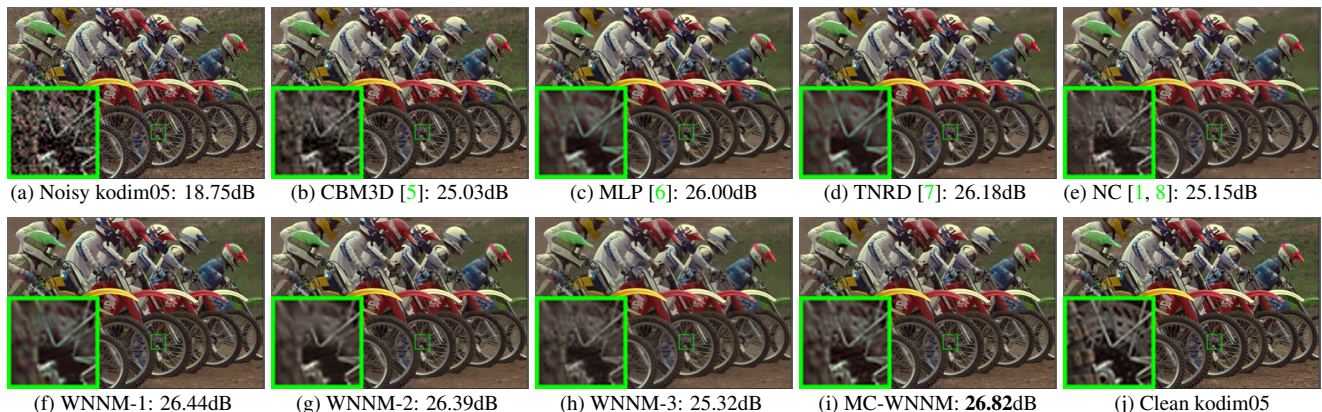


Figure 3. Denoised images of different methods on the image “kodim05” degraded by AWGN with different standard deviations of $\sigma_r = 40$, $\sigma_g = 20$, $\sigma_b = 30$ on R, G, B channels, respectively. The images are better to be zoomed in on screen.

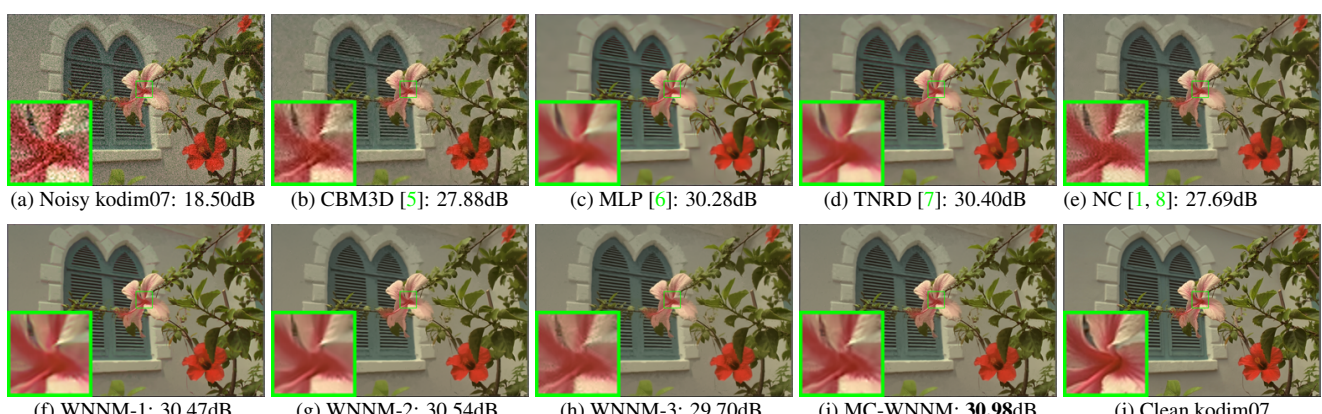


Figure 4. Denoised images of different methods on the image “kodim07” degraded by AWGN with different standard deviations of $\sigma_r = 40$, $\sigma_g = 20$, $\sigma_b = 30$ on R, G, B channels, respectively. The images are better to be zoomed in on screen.

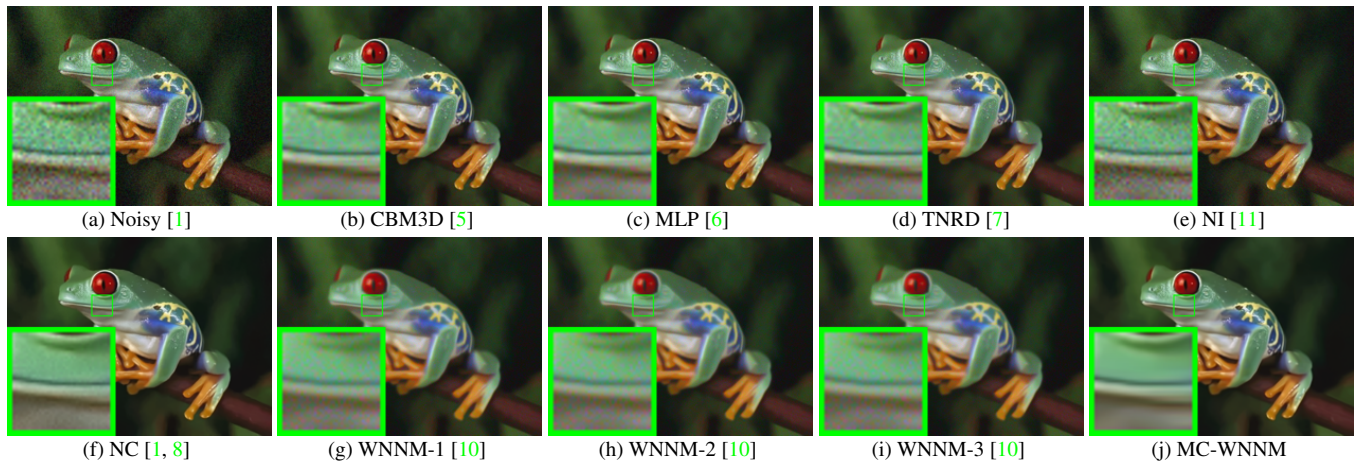


Figure 5. Denoised images of the real noisy image “Frog” [1] by different methods. The images are better to be zoomed in on screen.

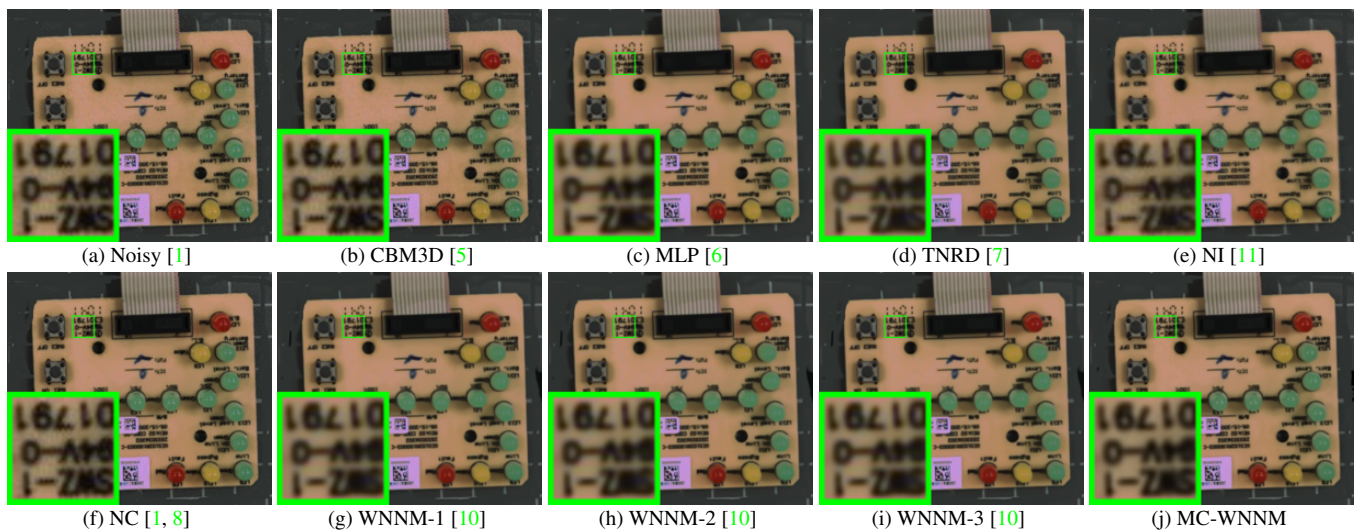


Figure 6. Denoised images of the real noisy image “Circuit” [1] by different methods. The images are better to be zoomed in on screen.

3. More visual comparisons of denoised images by different methods on the real noisy images of the dataset [1]

In this section, we give more comparisons of the state-of-the-art denoising methods on the dataset [1]. The real noisy images in dataset [1] have no “ground truth” images and hence we only compare the visual quality of the denoised images by different methods. As can be seen from Figures ??-??, our proposed method performs better than the competing methods.

4. More visual comparisons of denoised images by different methods on the real noisy images of the dataset [2]

In this section, we provide more comparisons of the proposed method with the state-of-the-art denoising methods on the 15 cropped real noisy images used in [2]. In this dataset, each scene was shot 500 times under the same camera and camera setting. The mean image of the 500 shots is roughly taken as the “ground truth”, with which the PSNR can be computed. As can be seen from Figures 11-??, in most cases, our proposed method achieves better performance than the the competing methods. This validates the effectiveness of our proposed external prior guided internal prior learning framework for real noisy image denoising.



Figure 7. Denoised images of the real noisy image “Woman” [1] by different methods. The images are better to be zoomed in on screen.

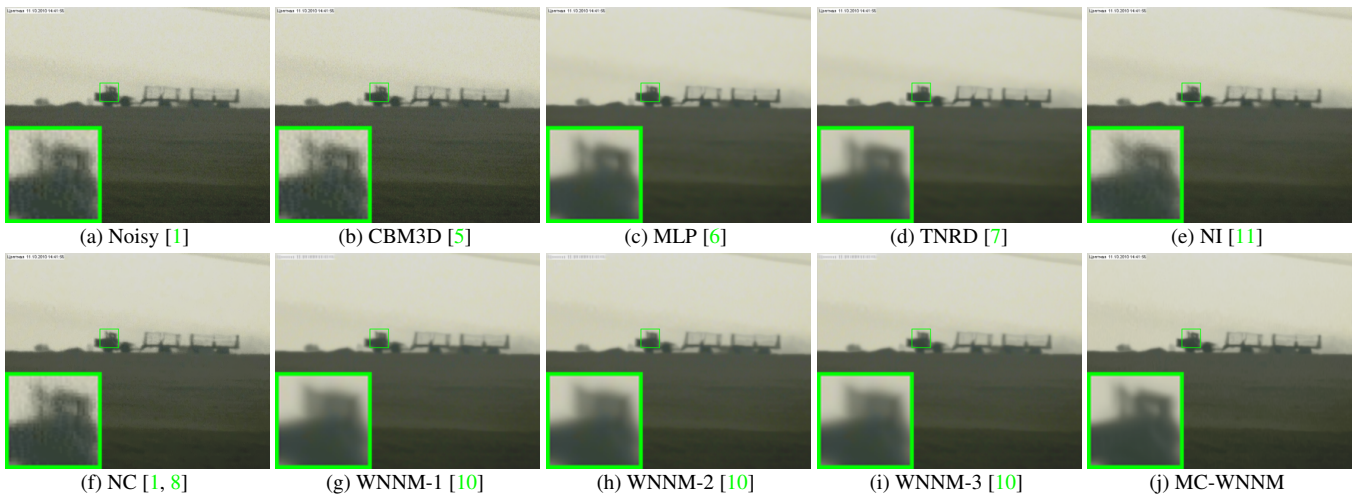


Figure 8. Denoised images of the real noisy image “Vehicle” [1] by different methods. The images are better to be zoomed in on screen.

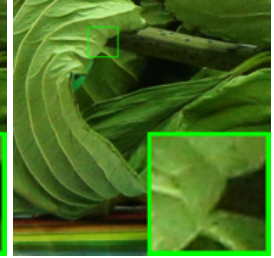
References

- [1] M. Lebrun, M. Colom, and J. M. Morel. The noise clinic: a blind image denoising algorithm. <http://www.ipol.im/pub/art/2015/125/>. Accessed 01 28, 2015. 1, 3, 4, 5, 6, 7, 8
- [2] S. Nam, Y. Hwang, Y. Matsushita, and S. J. Kim. A holistic approach to cross-channel image noise modeling and its application to image denoising. *IEEE Conference on Computer Vision and Pattern Recognition (CVPR)*, pages 1683–1691, 2016. 1, 5, 7, 8
- [3] C. Eckart and G. Young. The approximation of one matrix by another of lower rank. *Psychometrika*, 1(3):211–218, 1936. 1
- [4] S. Gu, Q. Xie, D. Meng, W. Zuo, X. Feng, and L. Zhang. Weighted nuclear norm minimization and its applications to low level vision. *International Journal of Computer Vision*, pages 1–26, 2016. 1
- [5] K. Dabov, A. Foi, V. Katkovnik, and K. Egiazarian. Color image denoising via sparse 3D collaborative filtering with grouping constraint in luminance-chrominance space. *IEEE International Conference on Image Processing (ICIP)*, pages 313–316, 2007. 3, 4, 5, 6, 7, 8
- [6] H. C. Burger, C. J. Schuler, and S. Harmeling. Image denoising: Can plain neural networks compete with BM3D? *IEEE Conference on Computer Vision and Pattern Recognition (CVPR)*, pages 2392–2399, 2012. 3, 4, 5, 6, 8
- [7] Y. Chen, W. Yu, and T. Pock. On learning optimized reaction diffusion processes for effective image restoration. *IEEE Conference on Computer Vision and Pattern Recognition (CVPR)*, pages 5261–5269, 2015. 3, 4, 5, 6, 7, 8

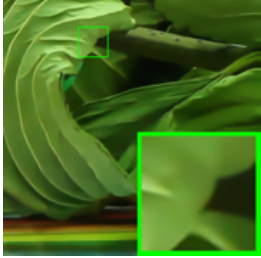
648



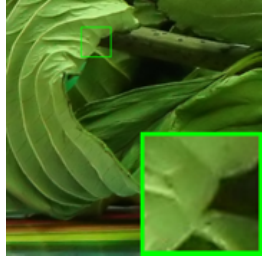
(a) Noisy [2]: 33.88dB



(b) CBM3D [5, 9]: 33.91dB



(c) TNRD [7]: 34.33dB

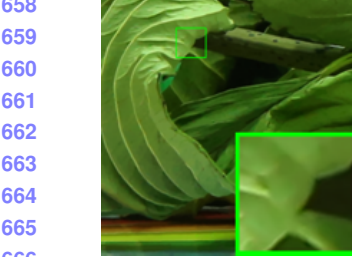


(d) NI [11]: 34.87dB



(e) NC [1, 8]: 35.69dB

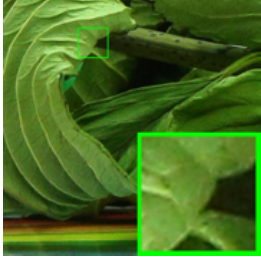
657



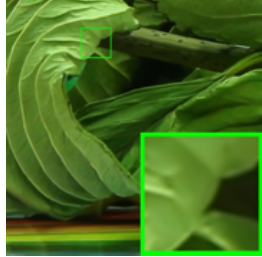
(f) CC [2]: 35.37dB



(g) WNNM-2 [10]: 33.88dB



(h) WNNM-3 [10]: 33.88dB



(i) Ours: 37.05dB



(j) Mean Image [2]

668

Figure 9. Denoised images of a region cropped from the real noisy image “Canon 5D Mark 3 ISO 3200 2” [2] by different methods. The images are better to be zoomed in on screen.

669

670



(a) Noisy [2]: 33.88dB



(b) CBM3D [5, 9]: 33.91dB



(c) TNRD [7]: 34.33dB

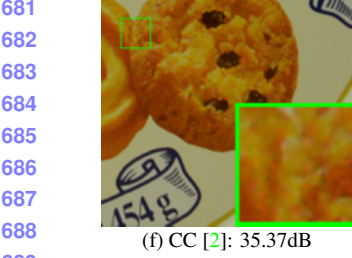


(d) NI [11]: 34.87dB



(e) NC [1, 8]: 35.69dB

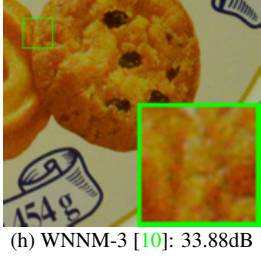
671



(f) CC [2]: 35.37dB



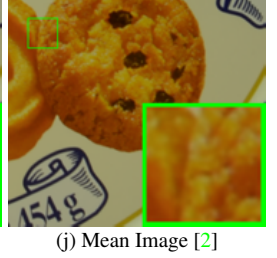
(g) WNNM-2 [10]: 33.88dB



(h) WNNM-3 [10]: 33.88dB



(i) Ours: 37.05dB



(j) Mean Image [2]

689

Figure 10. Denoised images of a region cropped from the real noisy image “Nikon D600 ISO 1600 2” [2] by different methods. The images are better to be zoomed in on screen.

690

691

692

693

- [8] M. Lebrun, M. Colom, and J.-M. Morel. Multiscale image blind denoising. *IEEE Transactions on Image Processing*, 24(10):3149–3161, 2015. 3, 4, 5, 6, 7, 8

694

695

- [9] K. Dabov, A. Foi, V. Katkovnik, and K. Egiazarian. Image denoising by sparse 3-D transform-domain collaborative filtering. *IEEE Transactions on Image Processing*, 16(8):2080–2095, 2007. 7, 8

696

697

698

699

700

701

- [10] S. Gu, L. Zhang, W. Zuo, and X. Feng. Weighted nuclear norm minimization with application to image denoising. *IEEE Conference on Computer Vision and Pattern Recognition (CVPR)*, pages 2862–2869, 2014. 5, 6, 7, 8

702

703

704

705

706

707

708

709

710

711

712

713

714

715

716

717

718

719

720

721

722

723

724

725

726

727

728

729

730

731

732

733

734

735

736

737

738

739

740

741

742

743

744

745

746

747

748

749

750

751

752

753

754

755

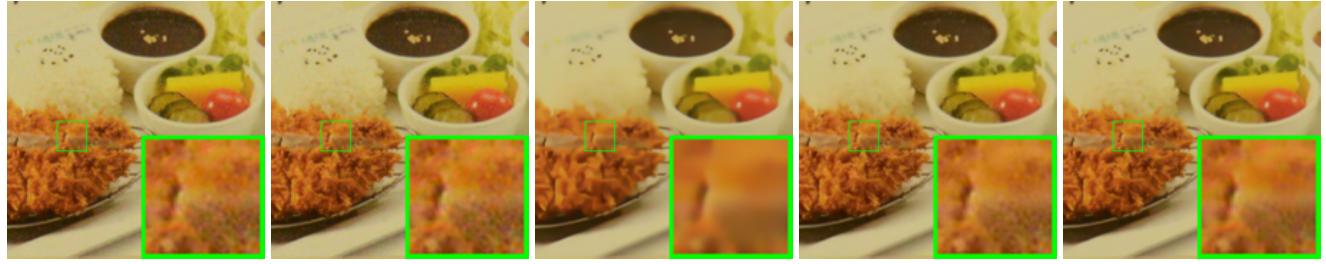
756
757
758
759760
761
762
763
764
765
766
767768
769
770
771
772
773
774
775
776

Figure 11. Denoised images of a region cropped from the real noisy image “Nikon D800 ISO 1600 2” [2] by different methods. The images are better to be zoomed in on screen.

777

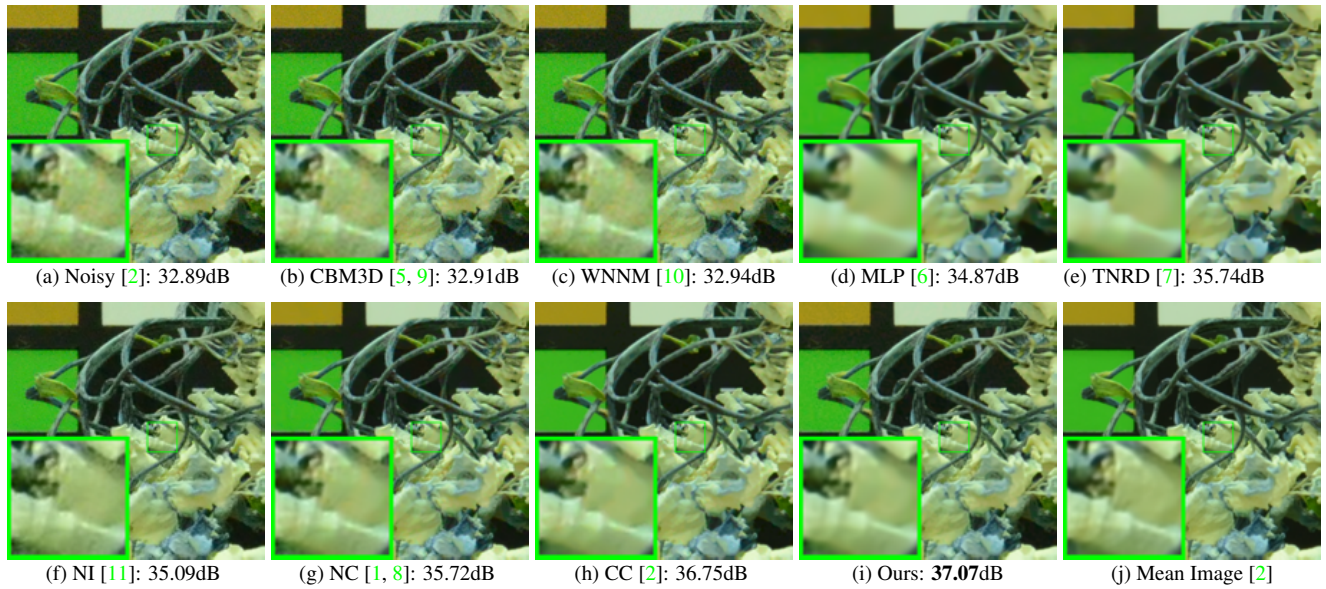
805
806

Figure 12. Denoised images of a region cropped from the real noisy image “Nikon D800 ISO 6400 2” [2] by different methods. The images are better to be zoomed in on screen.

807

808

809

810
811
812
813
814
815
816
817
818
819
820
821822
823
824
825
826
827
828
829
830831
832
833
834835
836
837
838
839840
841
842
843
844
845
846
847848
849850
851
852
853
854
855
856
857858
859
860
861
862
863